

PAPER

Early prediction of dementia using fMRI data with a graph convolutional network approach

To cite this article: Shuning Han *et al* 2024 *J. Neural Eng.* **21** 016013

View the [article online](#) for updates and enhancements.

You may also like

- [A COMPARATIVE STUDY OF LONG AND SHORT GRBS. I. OVERLAPPING PROPERTIES](#)
Ye Li, Bing Zhang and Hou-Jun Lü
- [THE AFTERGLOWS OF SWIFT-ERA GAMMA-RAY BURSTS. II. TYPE I GRB VERSUS TYPE II GRB OPTICAL AFTERGLOWS](#)
D. A. Kann, S. Klose, B. Zhang et al.
- [INVESTIGATING THE IMPACT OF OPTICAL SELECTION EFFECTS ON OBSERVED REST-FRAME PROMPT GRB PROPERTIES](#)
D. Turpin, V. Heussaff, J.-P. Dezalay et al.

The Breath Biopsy® Guide
Fourth edition

FREE

DOWNLOAD THE FREE E-BOOK

BREATH BIOPSY

OWLSTONE MEDICAL



PAPER

Early prediction of dementia using fMRI data with a graph convolutional network approach

RECEIVED
24 August 2023REVISED
27 November 2023ACCEPTED FOR PUBLICATION
12 January 2024PUBLISHED
29 January 2024Shuning Han^{1,2}, Zhe Sun^{3,*} , Kanhao Zhao⁴, Feng Duan⁵, Cesar F Caiafa^{6,9,*} , Yu Zhang^{4,7} and Jordi Solé-Casals^{1,8,*} ¹ Data and Signal Processing Research Group, University of Vic-Central University of Catalonia, Vic 08500, Catalonia, Spain² Image Processing Research Group, RIKEN Center for Advanced Photonics, RIKEN, Wako-Shi, Saitama, Japan³ Faculty of Health Data Science, Juntendo University, Urayasu, Chiba, Japan⁴ Department of Bioengineering, Lehigh University, Bethlehem, PA 18015, United States of America⁵ Tianjin Key Laboratory of Brain Science and Intelligent Rehabilitation, Nankai University, Tianjin, People's Republic of China⁶ Instituto Argentino de Radioastronomía-CCT La Plata, CONICET / CIC-PBA / UNLP, V. Elisa 1894, Argentina⁷ Department of Electrical and Computer Engineering, Lehigh University, Bethlehem, PA 18015, United States of America⁸ Department of Psychiatry, University of Cambridge, Cambridge CB20SZ, United Kingdom⁹ Tensor Learning Team, Riken AIP, Tokyo, Tokyo 103-0027, Japan

* Authors to whom any correspondence should be addressed.

E-mail: z.sun@juntendo.ac.jp, ccaiafa@fi.uba.ar and jordi.sole@uvic.cat**Keywords:** Alzheimer's disease, mild cognitive impairment, graph convolutional network, functional magnetic resonance imaging analysis, functional connectivity**Abstract**

Objective. Alzheimer's disease is a progressive neurodegenerative dementia that poses a significant global health threat. It is imperative and essential to detect patients in the mild cognitive impairment (MCI) stage or even earlier, enabling effective interventions to prevent further deterioration of dementia. This study focuses on the early prediction of dementia utilizing Magnetic Resonance Imaging (MRI) data, using the proposed Graph Convolutional Networks (GCNs). *Approach.* Specifically, we developed a functional connectivity (FC) based GCN framework for binary classifications using resting-state fMRI data. We explored different types and processing methods of FC and evaluated the performance on the OASIS-3 dataset. We developed the GCN model for two different purposes: (1) MCI diagnosis: classifying MCI from normal controls (NCs); and (2) dementia risk prediction: classifying NCs from subjects who have the potential for developing MCI but have not been clinically diagnosed as MCI. *Main results.* The results of the experiments revealed several important findings: First, the proposed GCN outperformed both the baseline GCN and Support Vector Machine (SVM). It achieved the best average accuracy of 80.3% (11.7% higher than the baseline GCN and 23.5% higher than SVM) and the highest accuracy of 91.2%. Secondly, the GCN framework with (absolute) individual FC performed slightly better than that with global FC generally. However, GCN using global graphs with appropriate connectivity can achieve equivalent or superior performance to individual graphs in some cases, which highlights the significance of suitable connectivity for achieving performance. Additionally, the results indicate that the self-network connectivity of specific brain network regions (such as default mode network, visual network, ventral attention network and somatomotor network) may play a more significant role in GCN classification. *Significance.* Overall, this study offers valuable insights into the application of GCNs in brain analysis and early diagnosis of dementia. This contributes significantly to the understanding of MCI and has substantial potential for clinical applications in early diagnosis and intervention for dementia and other neurodegenerative diseases. Our code for GCN implementation is available at: <https://github.com/Shuning-Han/FC-based-GCN>.

1. Introduction

Alzheimer's disease (AD) is a neurodegenerative dementia that progressively disrupts neurocognitive functions and poses a significant global health threat [1, 2]. The predominant manifestations of AD encompass diminished working and episodic memory, coupled with disruptions in executive function. Additional symptoms contain deficits in attention, visuospatial orientation, language, and neuropsychiatric symptoms [3]. The progression to AD usually includes three stages: (early) mild cognitive impairment (MCI), moderate dementia, and severe dementia. At present, there is no effective treatment for AD and symptomatic treatments for dementia could be effectual only in the early stage [4–6]. Therefore, it is imperative and essential to detect patients in the MCI stage, or even earlier, enabling effective interventions to prevent further deterioration of dementia.

In recent years, studies on magnetic resonance imaging (MRI) have shown substantial utility in understanding neuropathological mechanisms behind and clinical diagnosis of dementia [7]. MRI is based on the principle of absorption and emission of energy in radio-free range of electron magnetic spectrum, which can show the states of the whole brain non-invasively and safely. There are mainly two kinds of MRI: structural MRI (sMRI) reveals the detailed anatomical structure of the brain; and functional MRI (fMRI) depicts brain activity by detecting the temporal changes in brain hemodynamics. fMRI provides us significant information with a relatively high spatial resolution (2 mm isotropic) and medium temporal resolution (minutes) [8]. fMRI can be divided into two categories: task-evoked fMRI (tfMRI) which is collected while the subject is engaged in tasks, and resting-state fMRI (rfMRI) which is collected while the subject is resting. Spatial patterns of spontaneous neural activities and metabolism still exist in the resting-state brain, in which the functional connectivity (FC) between different brain regions can be deduced [9, 10]. FC reflects the brain functional organization, and its alterations are believed to be associated with brain psychiatric disorders [11].

Recently, graph theory and machine learning techniques have been widely applied in neuroscience for brain analysis and disease detection [9, 12–15]. Devika and Ramana Murthy Oruganti [16] developed a machine learning framework based on support vector machine (SVM) to diagnose neurological disorders using rfMRI. Helaly *et al* [17] used a CNN architecture for the early detection of AD with 2D and 3D structural brain. Bi *et al* [9] explored the functional brain network classification for AD

detection with deep features and extreme learning machine. Ebrahimi-Ghahnavieh *et al* [18] applied transfer learning for 2D convolutional neural networks (CNN) to sMRI for AD Detection.

Although the performance of deep learning methods, such as CNN, has been promising in data with Euclidean structure, it is difficult to extract representative features effectively from brain network graphs due to their irregular Euclidean structures [19, 20]. As a result, a new field of geometric deep learning, graph neural networks (GNNs), has emerged, which has given the possibility to effectively process signals in the non-Euclidean geometry of graphs. Recently more and more GNNs have been proposed and applied in brain MRI analysis and disorder detection [21, 22]. Parisot *et al* [23] introduced the spectral graph convolution network (GCN) with rfMRI and non-imaging data, representing populations as a sparse graph. This approach achieved an accuracy of 69.5% for autism spectrum disorder (ASD) detection on the ABIDE dataset and 77% for predicting MCI conversion on the ADNI dataset. Ktena *et al* [24] developed supervised Siamese GCN to evaluate the similarity between a pair of graphs and applied it to FC networks derived from rfMRI data in the ABIDE dataset for the purpose of ASD detection, resulting in an average accuracy of around 67%. Wang *et al* [25] presented an averaged global FC based GCN architecture for rfMRI analysis and applied it to the classification of ASD patients from NCs on the ABIDE dataset, achieving the best average accuracy with tenfold cross-validation at 70.7%. Tang *et al* [26] proposed an averaged FC based contrastive learning framework featuring an interpretable hierarchical signed graph representation learning model. This model was employed for AD prediction using rfMRI data from the OASIS dataset, achieving an accuracy of 77.51%. Lei *et al* [27] developed a multi-scale enhanced GCN integrating the diffusion tensor imaging (DTI) and rfMRI. This integrated model was applied to the ADNI dataset for detecting MCI, attaining an accuracy of 90.30%. Nevertheless, this model underwent testing on a relatively small cohort of 184 subjects, and awaits further validation. Despite these advancements, there is limited research focusing on the impact of different ways of calculating FC on brain analysis results. Moreover, the performance of GCN models in brain disorder detection remains less than satisfactory. In addition, there are currently few studies using MRI to detect the risk of MCI or dementia, i.e. to predict MCI or dementia before it is clinically diagnosed. This prognostic capability holds critical significance in impeding or decelerating the disease progression.

Taking the aforementioned into consideration, this study presents a state-of-art approach in the field

of neuroimaging based disease detection and prediction. The key highlights of this research are as follows:

A novel FC based GCN framework for disease detection using neuroimaging: We develop an innovative FC based GCN framework for binary classifications utilizing rfMRI data. The GCN framework is applied to two types of classification: (1) diagnosis of MCI by rfMRI classification of NCs and MCI; (2) prediction of dementia risk by classifying rfMRI of patients not clinically diagnosed with MCI, but exhibiting the potential for MCI, in comparison to the rfMRI of NCs.

Impact of FC: This study places special emphasis on understanding the effects of different FC types and processing methods on the GCN framework's performance. In this paper, FC is regarded as a graph and is considered in two aspects: on one side, we compare the difference of using the global FC matrix obtained from the training data versus the individual specific FC matrices of each rfMRI data; on the other side, we employ different processing methods for the FC matrices, and obtain the k nearest neighbor (k -NN) graph, the threshold graph, the top- p graph and the p -Minimum Spanning Tree (MST) graph.

Insightful Network Analysis: The study conducts an in-depth analysis of brain networks including self-network and between-network connectivity. This perspective enhances the clinical relevance and impact of this study's findings.

The rest of this paper is organized as follows. Section 2 describes the utilized dataset and methods. Section 3 presents the analysis results which are discussed in section 4. Finally, section 5 concludes this work.

2. Materials and methods

In this paper, we focus on implementing MCI diagnosis and dementia risk prediction with longitudinal rfMRI data, and analyze the effects of different FC on the classification results. In this section, we first introduce the dataset for classification and how labels are assigned. Then, we present the fMRI acquisition and preprocessing methods, how to get different FC, and finally the proposed GCN framework and the baseline methods used for comparison.

2.1. Data

Longitudinal rfMRI series are adopted to analyze the binary classification performance of the proposed GCN framework. We label the rfMRI samples into 3 classes: *NC*, *risking dementia (RD)*, and *MCI*, based on the relevant clinical assessments of the participants.

2.1.1. OASIS-3 dataset

The dataset from the Open Access Series of Imaging Studies (OASIS)-3 [28] (www.oasis-brains.org) is utilized to validate our proposed GCN framework. The dataset includes longitudinal fMRI, neuropsychological tests and clinical data of 1098 participants (605 cognitively normal, 493 in various stages of cognitive decline) aged 42–95 years. The clinical dementia rating (CDR) scale is adopted to assess the dementia status in the clinical data of OASIS-3 dataset: CDR 0 indicating normal cognitive function, CDR 0.5 indicating very mild impairment, CDR 1 indicating mild impairment, and CDR 2 indicating moderate dementia. All participants were required to have a $CDR \leq 1$ in the most recent clinical core assessment, and once a participant reached CDR 2, they were no longer eligible in the study.

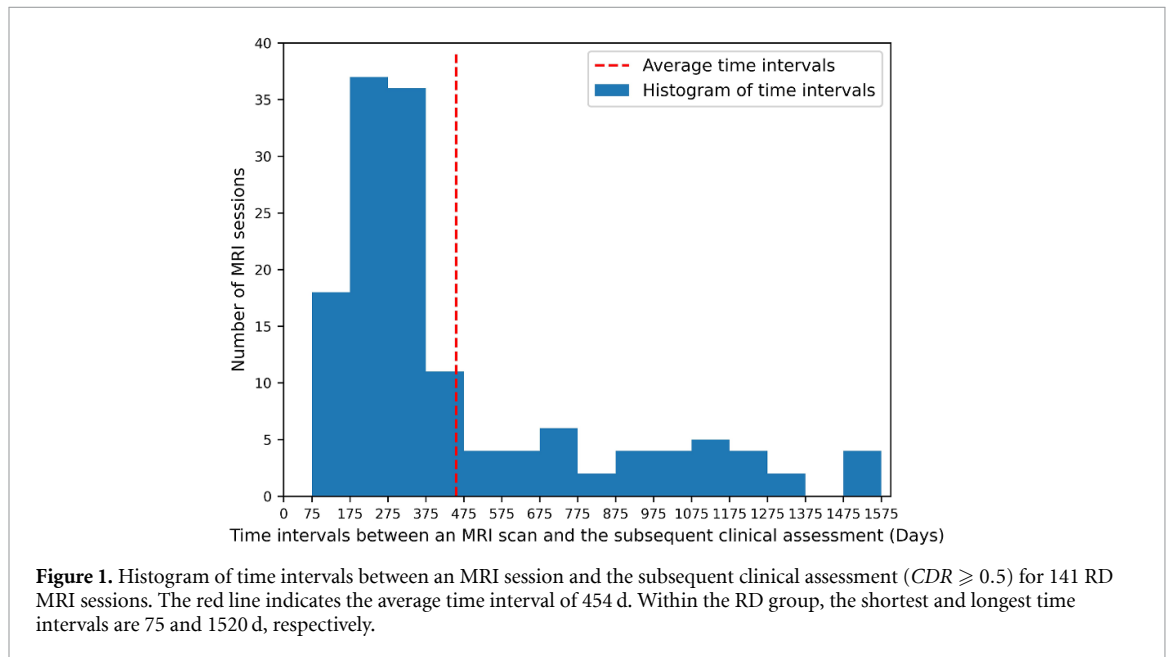
2.1.2. MRI sessions labeling

MRI sessions can be labeled according to the associated CDR values. However, clinical assessments were conducted on different days from the neural imaging scans, as illustrated in figure 1, and the time gap between the MRI scan and clinical assessment may exceed 1 year in the longitudinal OASIS-3 dataset. In this current work, MRI sessions are categorized into three groups: *NC*, *RD*, and *MCI*. An MRI session is labeled as *NC*, if all of the clinical assessment results of the corresponding subject are $CDR = 0$ in the recorded data; an MRI session is labeled as *RD*, if the latest clinical assessment result before the scan is $CDR = 0$ and the subsequent clinical assessment result switches to $CDR \geq 0.5$, which indicates that the subject transitioned to a dementia status during the two consecutive clinical assessments, and that they are at risk of dementia when undergoing the MRI scan; an MRI scan is labeled as *MCI*, if the preceding and subsequent clinical assessment results are both $CDR \geq 0.5$. As a result, a total of 1831 MRI sessions from 500 subjects are labeled as *NC*; 141 MRI sessions from 219 subjects are labeled as *RD*; 503 MRI sessions from 68 subjects are labeled as *MCI*. The mean ages of subjects *NC*, *RD* and *MCI* are all approximately 68 years. The details are shown in table 1).

In addition, the date differences of the 141 *RD* MRI sessions from the date of MRI scan to the next clinical assessment date were calculated. As shown in figure 1, the shortest, longest and mean date difference in the *RD* group is 75, 1520 and 454 d respectively. The long time intervals between the MRI scan and the subsequent clinical assessment suggest the need to label as *RD* the MRI session that falls between two clinical assessments with changing CDR results.

Table 1. A statistic of the labeled fMRI.

Label of fMRI	CDR	Number of fMRI sessions	Number of subjects	Average age of subjects at each MRI scan
NC	All CDR results of the subject are 0.	1831	500	68.62 (± 3.57)
RD	The latest clinical assessment result before the scan is $CDR = 0$ and the subsequent assessment switches to $CDR \geq 0.5$.	141	68	68.98 (± 4.43)
MCI	The preceding and subsequent clinical assessment results are both $CDR \geq 0.5$.	503	219	68.04 (± 4.23)



2.2. Methods

We are focused on implementing the diagnosis of MCI and risk prediction of dementia by the proposed GCN framework. The GCN framework is based on FC of the brain for binary classification. Meanwhile, we analyze how different kinds of FC impact the classification results by using different processing methods for FC and using global or individual FC.

This part presents a thorough exposition on the fMRI acquisition and pre-processing methods, as well as the different FC processing methods. The proposed GCN framework and the baselines are then described in detail.

2.2.1. fMRI acquisition and preprocessing

For subjects in each run, the fMRI data were scanned in resting state for 6 min (164 volumes) using 16-channel head coil of scanners with parameters: $TR = 2$ s, $TE = 27$ ms, $FOV = 240 \times 240$ mm, and $FA = 90^\circ$. The acquired initial rfMRI data were preprocessed using the well-established fMRIPrep pipeline [29]. The T1-weighted (T1w) image was corrected for intensity non-uniformity and then stripped

skull. Spatial normalization was done through non-linear registration, with the T1w [30]. Using FSL, brain features such as cerebrospinal fluid, white matter, and grey matter were segmented from the reference, brain-extracted T1 weighted image [31]. The fieldmap information was used to correct distortion in low-frequency and high-frequency components of fieldmap. Then, a corrected echo-planar imaging reference was obtained from a more accurate co-registration with the anatomical reference. The blood-oxygenation-level-dependent (BOLD) reference was then transformed to the T1-weighted image with a boundary-based registration method, configured with nine degrees of freedom to account for distortion remaining in the BOLD [32]. Head-motion parameters (rotation and translation parameters of volume-to-reference transform matrices) were estimated with MCFLIRT (FSL). BOLD signals were slice-time corrected and resampled onto the participant's original space with head-motion correction, susceptibility distortion's correction, and then resampled into standard space, generating a preprocessed BOLD run in MNI152NLin2009cAsym space. Automatic removal of motion artifacts using

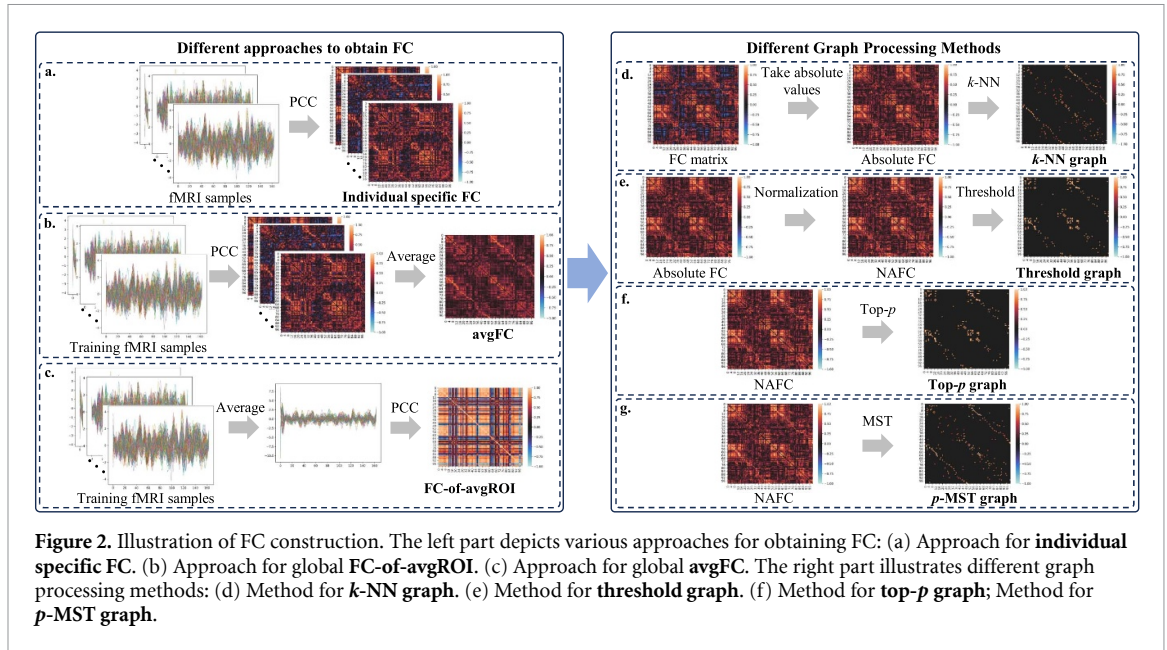


Figure 2. Illustration of FC construction. The left part depicts various approaches for obtaining FC: (a) Approach for **individual specific FC**. (b) Approach for global **FC-of-avgROI**. (c) Approach for global **avgFC**. The right part illustrates different graph processing methods: (d) Method for **k-NN graph**. (e) Method for **threshold graph**. (f) Method for **top-p graph**; Method for **p-MST graph**.

independent component analysis (ICA-AROMA) [33] was performed on the preprocessed BOLD time-series on MNI space after removal of non-steady-state volumes and spatial smoothing with an isotropic Gaussian kernel of 6 mm full-width half-maximum (FWHM).

2.2.2. FC construction

The preprocessed BOLD-level rfMRI series are averaged into 100 ROIs defined from Schaefer atlas [34] and then standardized by z-score. Finally, the dimension of each fMRI session is 164×100 (100 regions with a length of 164 time samples each). The brain FC can be obtained from rfMRI and modeled as graphs, which describe the statistical time-series correlations between brain regions of interest (ROIs). In this paper, we analyze how different types of FC influence the prediction results. The difference of FC is reflected in two aspects, as illustrated in figure 2: one is the different FC matrices, individual specific FC matrices obtained from each fMRI data versus global FC matrix obtained from the training data, for both training and testing data; the other is the different processing methods used to obtain the FC matrices.

- Pearson correlation coefficient (PCC)

To obtain the FC matrices of ROIs, the PCC between the fMRI time series of each pair of brain regions is calculated as

$$\begin{aligned} \text{PCC}(x, y) &= \frac{\text{cov}(x, y)}{\sigma_x \sigma_y} \\ &= \frac{\sum_{i=1}^n (x_i - \bar{x})(y_i - \bar{y})}{\sqrt{\sum_{i=1}^n (x_i - \bar{x})^2} \sqrt{\sum_{i=1}^n (y_i - \bar{y})^2}} \end{aligned} \quad (1)$$

where x and y are the time series of two brain regions obtained from fMRI data; n is the time series length; $\text{cov}(x, y)$ is the covariance of x and y ; σ is the standard deviation of a variable; \bar{x} and \bar{y} are the mean value of x and y respectively [9].

The set of PCC values forms the whole-brain FC matrix for each subject, characterized by symmetry and a theoretical range from -1 to 1 : a value close to -1 indicates anti-correlation between the pair of the time series; a value close to 1 indicates strong correlation between the pair of the time series [35, 36]. In practice, the original FC matrix typically does not contain values equal to -1 , and its diagonal elements equal to 1 . However, we uniformly assign zero values to the diagonal elements of the FC matrices, facilitating subsequent normalization processing. There are 100 regions in the ROIs, thus the shape of FC matrix is 100×100 .

- Approaches for obtaining different types of FC matrices from training data

The left side of figure 2 shows the approaches for obtaining different types of FCs. Individual specific FC matrices can be derived from each fMRI data by directly calculating the PCC, as shown in figure 2(a). Meanwhile, a global FC matrix for training and test fMRI samples is generated from training samples by different approaches: In one approach, a global FC matrix is obtained from the standardized average data of the training fMRI samples (denoted as **FC-of-avgROI**), as shown in figure 2(b). In the other approach, we consider the average PCC of all PCC matrices from the training fMRI samples (denoted as **avgFC**) as the global FC matrix, as shown in figure 2(c).

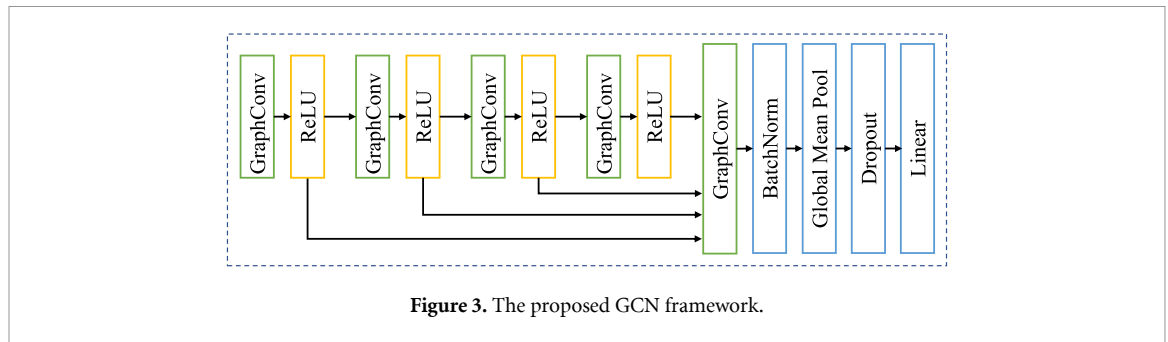


Figure 3. The proposed GCN framework.

It should be noted that: (1) all the matrix averaging operations are across subjects; (2) the second approach of the global FC was also used in the baseline; (3) the individual FC and the two types of global FC, derived through PCC computation, undergo further processing using the methods outlined in the right part of figure 2 ‘**Different graph processing methods**’.

- Different graph processing methods

To analyze how different types of graphs impact the classification results of GCN, we apply different processing methods to the FC matrix obtained from the fMRI time series, as shown in the right part of figure 2. In the first method, we take the k largest values in each row of the FC matrix with absolute values as the **k -NN graph**, as shown in figure 2(d). In the second method, the absolute FC undergoes Min–Max normalization, scaling its values to the range $[0 - 1]$ for consistent thresholding, referred to as normalized absolute FC (NAFC). Subsequently, thresholding is applied on the NAFC matrix (denoted as **threshold graph**), as illustrated in figure 2(e).

To further explore the effect of graph connectivity on our model, we implement two additional methods. The third method (figure 2(f)) constructs the **top- p graph**, which is the symmetric matrix of the top- p percentage values of the upper triangular NAFC matrix, without considering whether the graph is fully connected or not. In the fourth method (figure 2(g)), the fully connected **p -MST graph** is generated based on MST [37]. MST is a unique acyclic subgraph that connects N nodes with $(N-1)$ edges. By first finding the MST and adding edges to this backbone, we ensure that resulting graphs will be fully-connected [38]. Since the p -MST graph is fully connected, the smallest percentage (p) of MST graph in the upper triangular matrix is $(N - 1)/[(N - 1)N/2] = 2\%$, where N equals 100.

2.2.3. Graph neural network (GNN)

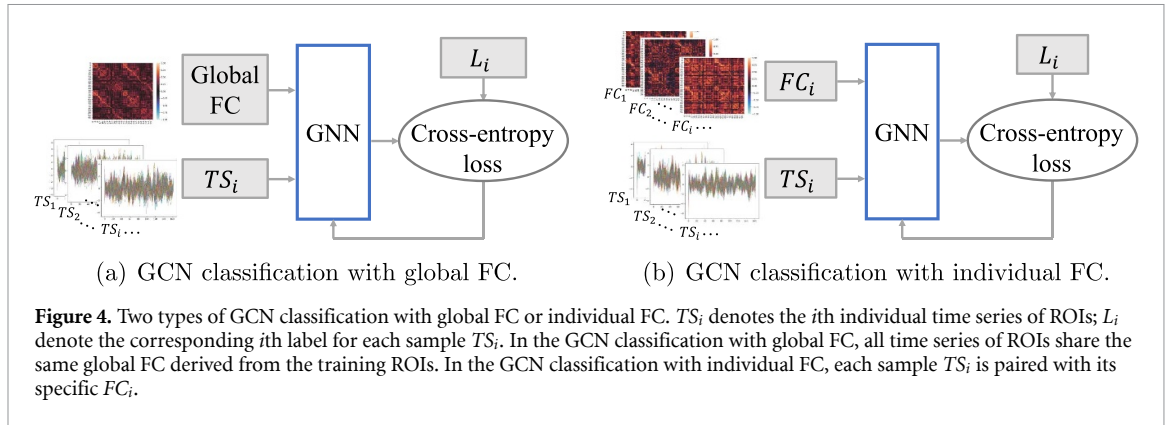
Graphs [39] are a kind of non-Euclidean data structure composed by a set of nodes and edges, where nodes represent objects and edges represent the relationship between objects. Brain FC can be modeled as graphs, where nodes represent ROIs and edges

correspond to correlations in activity between these ROIs [40–42]. GNNs [21, 43] have recently become a widely used machine learning tool in graph analysis due to their persuasive performance. The GNN architectures effectively combine node features and graph topology to build distributed node representations [44]. In this work, we develop a novel framework of GNN for binary classification of different sorts of fMRI data, in which the rfMRI time series of brain ROIs are directly regarded as the node features and the FC as the graph topology.

- The proposed GCN

The proposed GCN framework is implemented on the basis of the Pytorch Geometric (PyG) library [45], which contains various GNN models and graph pre-processing methods to easily build and train GNNs. The designed GCN framework (shown in figure 3) contains five graph convolutional layers based on GraphConv [46]. The nonlinear activation function Rectified Linear Unit (ReLU) [47] layer defined as $f(x) = \max(0, x)$ follows after each of the first 4 graph convolutional layers (GCLs), and the input of the last GCL layer is the outputs of the first 4 layers. The fifth GCL includes a batch normalization level to make the GCN framework faster and more stable. Then the global mean pool or global average pool is followed to avoid overfitting and make the framework more robust. To further avoid overfitting, we applied a dropout layer in which output data are randomly set to zero with a certain probability.

In the proposed GCN framework, the Adam algorithm [48] is used as the optimizer, and the cross-entropy loss is performed as the loss function. The proposed GCN framework is applied for two kinds of classification with global FC or individual FC, illustrated in figure 4. In the GCN classification with global FC, see figure 4(a), the inputs of the GCN framework consist of individual time series of ROIs, each accompanied by the same shared global FC derived from the training ROIs, as described in ‘**Approaches for obtaining different types of FC matrices from training data**’. Additionally, the model is provided with the corresponding labels for each sample. On the other hand, in the GCN classification with individual FC, depicted in figure 4(b), the



inputs comprise individual time series of ROIs, each paired with its specific FC generated from the respective ROI. Corresponding labels for each sample are also included.

- Baselines

To provide a basis for comparison, we adopt two baselines: the Support Vector Machine (SVM) using the radial basis function (RBF) kernel [49], and the GCN architecture for fMRI analysis developed by Wang *et al* [25] in 2021.

The baseline GCN architecture with avgFC consisted of 5 convolutional layers, one recurrent neural network (RNN) layer and a Softmax layer. In the baseline paper, the GCN was applied for ASD classification and achieved the best average accuracy of 70.7% (max 79.0%, min 66.7%) when $k = 3$ (among 3, 5, 10, and 20) with 10-fold cross validation.

We reimplement the baseline GCN architecture and apply it to the OASIS-3 dataset using all recommended parameters from the original paper. In the current study, a 10-fold cross validation strategy is adopted to evaluate the performance of the GCN framework which is set to be the same when applying the baseline method to OASIS-3 dataset.

3. Results

We validate the effectivity of the proposed GCN framework on OASIS-3 dataset for the diagnosis of MCI and risk prediction of dementia based on different kinds of FC with rfMRI series of ROIs. In this section, we first present the configurations of the proposed GCN framework. Then, we provide all the classification results: (1) *MCI vs. NC* classification results; (2) *RD vs. NC* classification results.

3.1. Configurations

We used the labeled rfMRI data from the OASIS-3 dataset as described in section 2.1. The shape of each rfMRI series is 164×100 . To maintain the data balance, only 503 randomly selected NC and MCI rfMRI samples, respectively, are used for MCI detection; and 141 randomly selected NC and RD rfMRI samples,

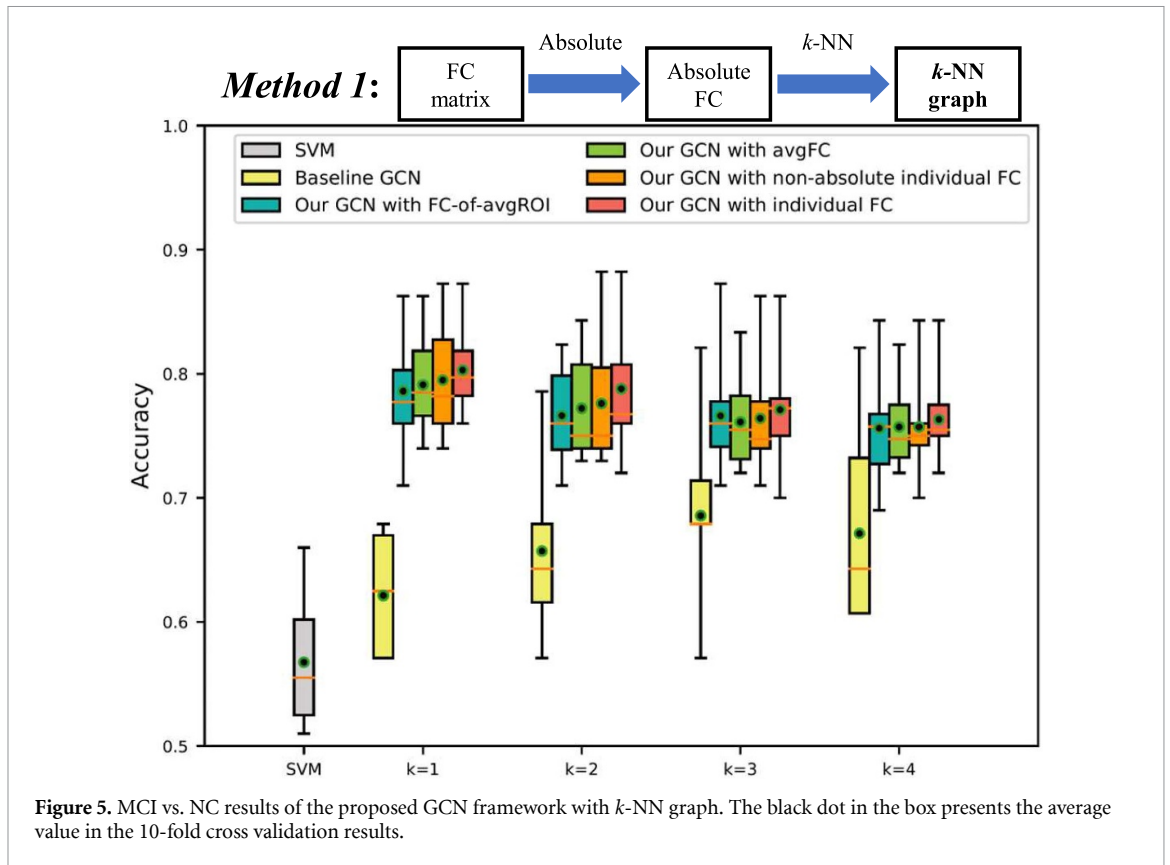
respectively, are used for MCI risk prediction. 10-fold cross validation method is used to evaluate the designed GCN framework on OASIS-3 dataset. To assess the impact of variations in the FC matrix on the outcomes, we varied the number of nearest neighbors k (1, 2, 3, and 4) and the threshold value (0.7, 0.8, 0.9, 0.95, and 0.99) for FC matrix processing. From section 3.2.2, it is observed that when $threshold \leq 0.9$, there is a consistent trend of increasing accuracy with threshold increments. We are interested in exploring the impact of higher thresholds on the outcomes and we specifically examine the threshold of 0.99 as an extreme case.

Code of the proposed GCN framework is implemented based on Python, and the GCN structure is realized by PyTorch based on PyG. In our experiment, each convolutional layer is designed with an output dimension of 128 to effectively capture intricate patterns while considering computational constraints. The choice of a learning rate is a delicate balance: a higher value risks overshooting the optimal solution, whereas a lower value may lead to slow convergence or entrapment in local minima. After careful consideration, we set the learning rate to 0.001. To prevent overfitting and encourage the learning of robust features and the generalization of GCN, a dropout rate of 0.5 is employed. The model undergoes training for 100 epochs to attain optimal accuracy. Additionally, a small batch size of 8 is chosen to expedite convergence and minimize memory usage.

The brain networks of different global graphs in one fold are visualized with Brainnet viewer [50]. The brain networks are grouped into seven canonical functional networks defined by the 7 Yeo networks [51]: visual network (VIS), somatomotor network (SMN), dorsal attention network (DAN), ventral attention network (VAN), limbic network (LIM), frontoparietal control network (FPC), default mode network (DMN).

3.2. MCI vs. NC classification results

As stated before, in order to better understand the impact of different FC, the proposed GCN utilizes the graphs of global FC (avgFC or FC-of-avgROI) or



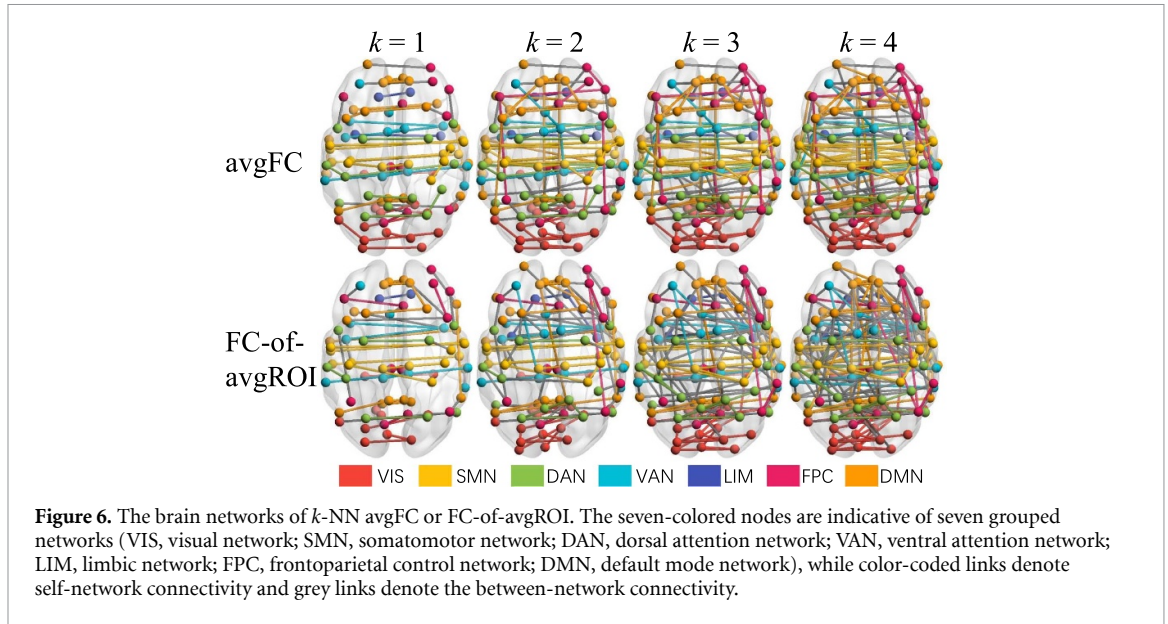
individual FC, and then the graphs are processed as **$k\text{-NN}$ graph, threshold graph, top- p graph, $p\text{-MST}$ graph**, respectively.

3.2.1. Results of GCN with $k\text{-NN}$ graph

We implement the MCI vs. NC classification of the proposed GCN with $k\text{-NN}$ graphs obtained from individual FC, non-absolute individual FC, global FC of avgFC and FC-of-avgROI. Especially, we also utilize the non-absolute individual FC here to demonstrate the superiority of GCN with absolute FC over that with non-absolute FC. It should be noted that absolute FC are used as the default in this article. We compare the performance of our proposed GCN with the baseline GCN framework and SVM method. The experimental results are shown in figure 5, which illustrates that: (1) The proposed GCN outperforms both the baseline GCN (best average accuracy of 68.6% when $k=1$) and SVM (average accuracy of 56.8%) in terms of accuracy. Our proposed GCN with $k\text{-NN}$ graphs achieves the best average accuracy of 80.3% with absolute-individual FC when $k=1$. (2) The proposed GCN with $k\text{-NN}$ graphs exhibits differently compared to the baseline GCN. While the accuracy of the baseline GCN increase as k increase and achieve the best average accuracy at $k=3$ (the same as in ASD classification in the baseline paper), our proposed GCN's performance with individual or global FC declines as k increases. (3) The proposed GCN with absolute individual FC performs slightly

better than that with the non-absolute individual FC. (4) Our proposed GCN with individual FC performs slightly better than that with global FC. The use of global avgFC or FC-of-avgROI exhibits negligible differences for the proposed GCN with $k\text{-NN}$ graphs.

Brain networks of $k\text{-NN}$ graphs of avgFC or FC-of-avgROI are displayed as figure 6. It is important to note that the $k\text{-NN}$ graphs are non-symmetrical matrix and cannot guarantee the full connectivity. In this figure, there are only 50 and 45 edges in avgFC and FC-of-avgROI as $k=1$, respectively. From the brain networks, it can be observed that: (1) Increasing k leads to more edges in both avgFC and FC-of-avgROI brain networks. This highlights an important finding that excessive connectivity can have a detrimental effect on improving classification performance, which is evidenced by the diminishing performance results as the number of connectivity (k) increases. (2) The brain networks of $k\text{-NN}$ avgFC and FC-of-avgROI show little difference for each value of k , which can explain the negligible difference of the accuracy between avgFC and FC-of-avgROI with same k . (3) The brain networks of avgFC involve a slightly larger number of ROIs than FC-of-avgROI when $k=1, 2$, and the average accuracy of GCN with avgFC are marginally higher than that of GCN with FC-of-avgROI. This finding illustrates that graphs involving a greater number of nodes may contain more valuable information for GCN classification.



3.2.2. Results of GCN with *threshold graph*

The MCI vs. NC classification performances of the proposed GCN with threshold graph derived from individual FC, global FC of avgFC or FC-of-avgROI are reported in figure 7. It can be observed that: (1) As the threshold value increases, the accuracy of GCN with FC-of-avgROI performs differently from that of GCN with individual FC or avgFC. (2) The average accuracy of GCN with FC-of-avgROI graphs are notably lower compared to that of GCN with individual FC or avgFC as $threshold \leq 0.95$, and then exhibits a significant rise when the threshold reaches 0.99. (3) The average accuracy of GCN with individual and avgFC graphs show a gradual increase and attain an optimal average accuracy at $threshold = 0.95$ and $threshold = 0.90$, respectively. Nonetheless, the accuracy of both decrease when $threshold = 0.99$. (4) Sometimes, the GNN with global FC achieves superior performance compared with GNN using individual FC. Overall, the proposed GCN with threshold graphs achieves the best average accuracy of 80.0% (max 88.2%, min 74.0%) with FC-of-avgROI graphs when $threshold = 0.99$.

The brain networks of avgFC and FC-of-avgROI with different threshold values are displayed in figure 8. It can be observed that: (1) Increasing threshold results in fewer edges in both networks. However, FC-of-avgROI contains much more edges than avgFC when $threshold > 0.7$. When few edges remain in the graph, there are self-network edges of SMN, DMN, FPC, and VIS in avgFC ($threshold = 0.9$); while, there are both self-network and between-network edges of SMN and VAN in FC-of-avgROI ($threshold = 0.99$). (2) The GCN with global FC that have very few edges in the graph obtained a higher average accuracy, which emphasizes the observation in k -NN graphs that excessive connectivity can negatively affect classification

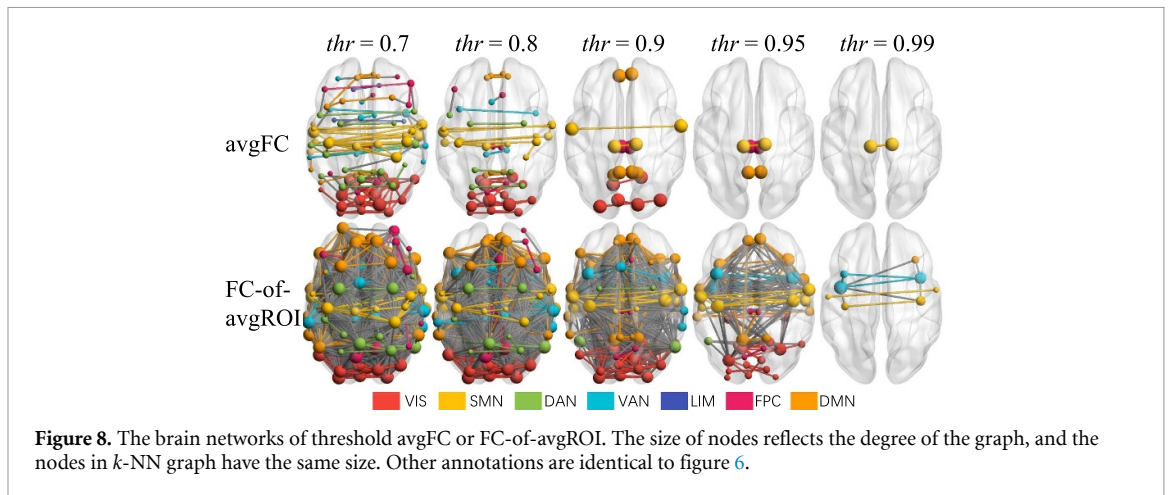
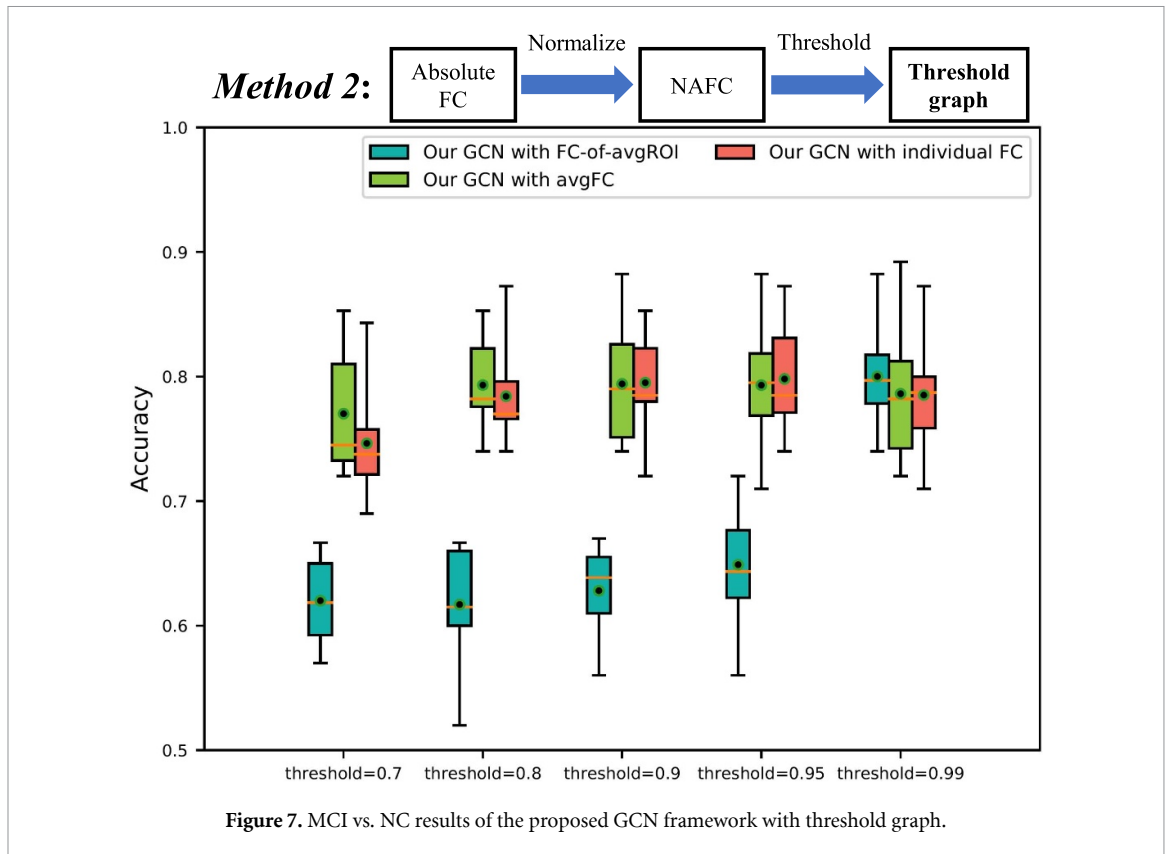
performance. (3) The slight decrease in average GCN accuracy with avgFC when there is only one edge left ($threshold = 0.99$) shows that a minimum number of edge information can cause a slight decrease in accuracy, although the ROI series contain a large amount of information. Furthermore, with suitable connectivity, the GNN with global FC can perform better than GNN with individual FC. These findings highlight the significance of suitable edge information for achieving performance, rather than the threshold itself.

3.2.3. Results of GCN with the *top-porp-MST graph*

To further investigate the impact of graph edges on GCN classification, we conduct a contrasting experiment of top- p or p -MST graphs while maintaining the same percentage p of edges in the graph. For clear comparison, we place the results of the two in the same figure 9. It can be observed that:

(1) Among the GCN classifier results with top- p graphs, GCNs with avgFC or individual FC achieve reasonable average accuracy as $p \leq 1.2\%$ and exhibit extremely strong robustness as p increases; GCNs with FC-of-avgROI achieve reasonable average accuracy as $p \leq 0.8\%$, slightly higher as $p \leq 0.4\%$ and significantly lower as $p \geq 1.0\%$. However, when $p \leq 0.1\%$, the average accuracy of all GCNs with individual FC, avgFC or FC-of-avgROI slightly decrease. Furthermore, it can be observed that all the GCN models with the three types of graphs show higher stability within the $0.2\% \leq p \leq 0.8\%$ range, as evidenced by the shorter difference between maximum and minimum values.

Optimal average accuracy of GCN with the three types of top- p graphs are: 79.8% at $p = 0.3\%$ (FC-of-avgROI); 79.2% at $p = 1.0\%$ (avgFC), 80.3% at $p = 0.2\%$ (individual FC). Particularly, the proposed GCN achieves the best accuracy 91.2% at $p = 2.2\%$ (individual FC).

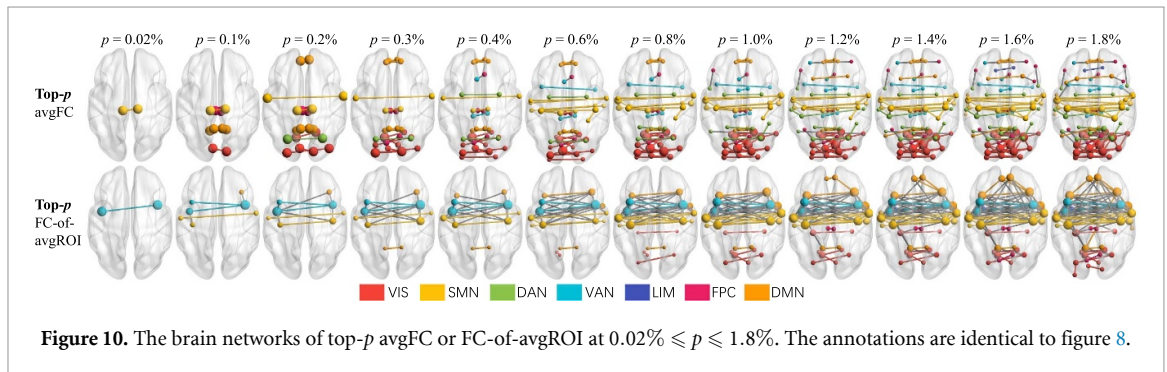
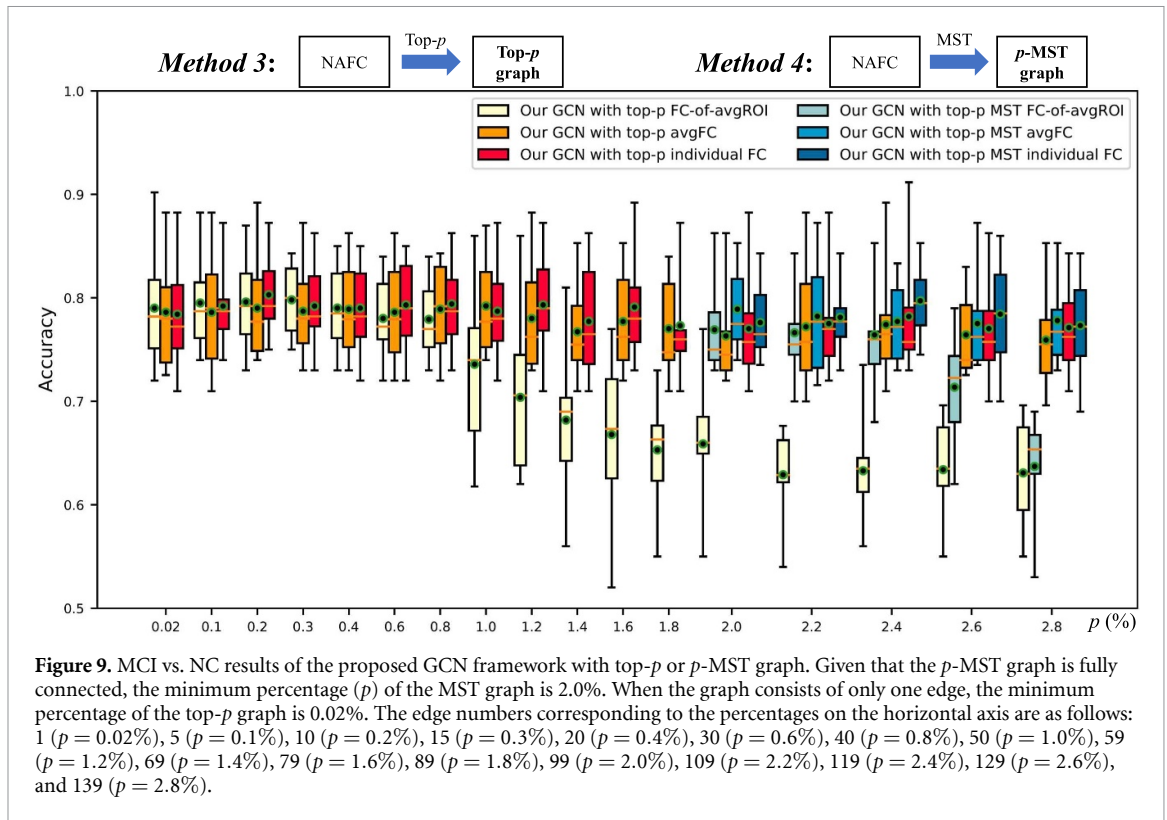


(2) Among the GCN classifier results with p -MST graphs, GCN with individual FC or avgFC achieves higher average accuracy and better robustness compared to GCN with FC-of-avgROI. Both the average accuracy of GNN with avgFC and FC-of-avgROI decrease as p increase, but the later exhibits a more significant decline. Optimal average accuracy of GCN with the three types of p -MST graphs are: 76.9% at $p = 2.0\%$ (FC-of-avgROI); 78.9% at $p = 2.0\%$ (avgFC); 79.7% at $p = 2.4\%$ (individual FC).

(3) By comparing, it is evident that utilizing fully-connected MST graphs in GCN yields better performance than top- p graphs with an equivalent edge percentage, as evidenced by the higher average

accuracy and shorter difference between maximum and minimum values. Moreover, the performance of GCN with individual FC or avgFC shows greater robustness as p increases compared to FC-of-avgFC. Additionally, the performance of GCN with individual FC is superior than that of GCN with global FC generally. Nevertheless, with appropriate edge information, GCN with global FC can perform as good as GCN with individual FC.

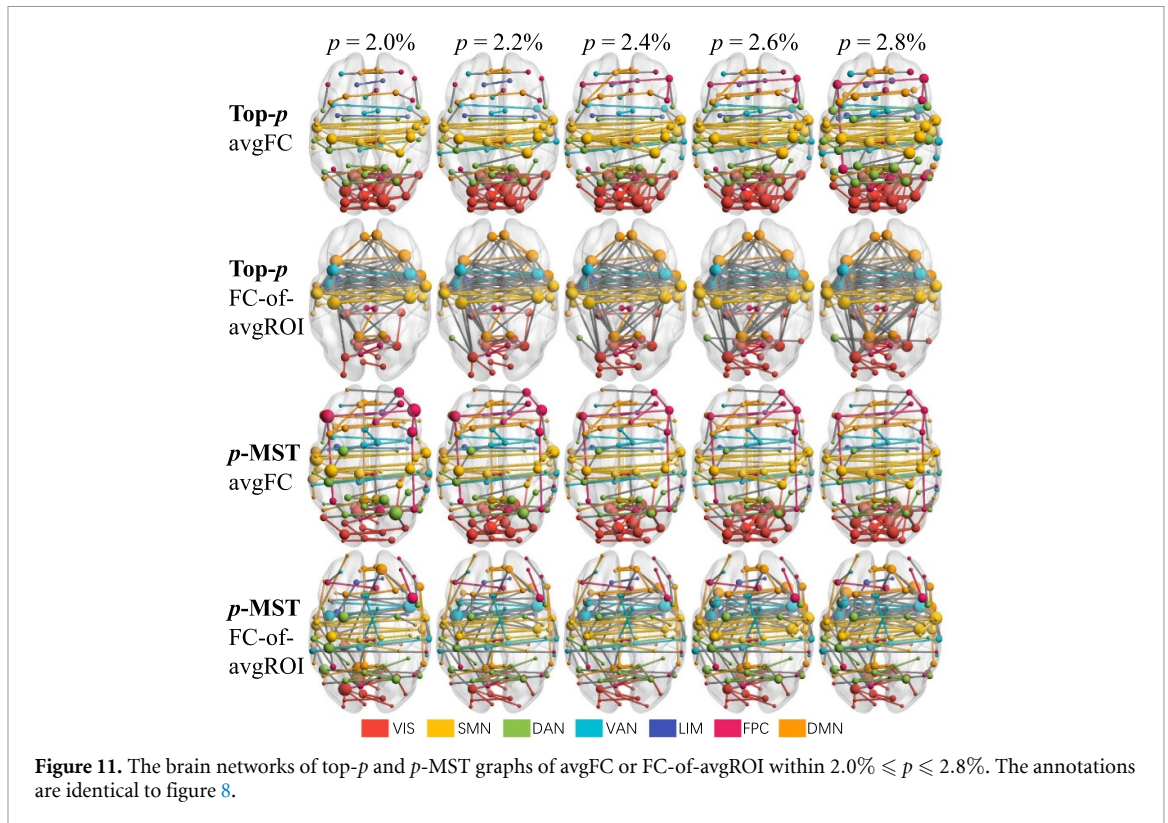
Figure 10 displays brain networks with top- p avgFC or FC-of-avgROI within the $0.02\% \leq p \leq 1.8\%$ range. For comparison, the brain networks shown in figure 11 exhibit both top- p and p -MST graphs of avgFC or FC-of-avgROI within $2.0\% \leq p \leq 2.8\%$.



(1) From figure 10, it can be found that, as p increases, the top- p avgFC graphs have more self-network connectivity in VIS and SMN, while the top- p FC-of-avgROI graphs have more between-network connectivity in VAN and SMN. Furthermore, the top- p avgFC graphs display more types of grouped brain networks (ROIs) and more self-network edges than top- p FC-of-avgROI as $p \geq 0.1\%$. The top- p avgFC with more types of brain networks (ROIs) and self-network connectivity (especially in VIS) contains more valuable information for GCN classification, while the top- p FC-of-avgROI with more between-network connectivity may contains useless information. These could explain why the performance of GCN with avgFC is enhanced as compared to GCN with FC-of-avgROI at higher values of $p > 0.6\%$. Specially, the average accuracy of GCN with FC-of-avgROI are marginally higher than that of GCN with

avgFC when $p \leq 0.4\%$. This demonstrates that self-network connectivity of VAN and SMN may play a more significant role in GCN classification.

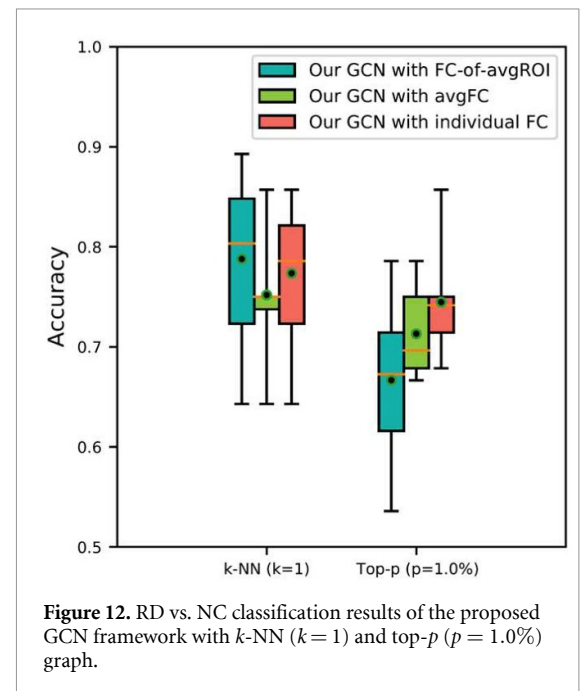
(2) Compared with top- p graphs, MST graphs are fully connected and contain more graph information as shown in figure 11. This may explain that the average accuracy of GCN with MST graph are consistently higher than that of GCN with corresponding top- p graph. Notably, a comparison between p -MST avgFC and p -MST FC-of-avgROI graphs reveals that the former has more self-network connectivity (especially in VIS) and fewer between-network connectivity, despite both containing all the ROIs. Besides, GCNs with p -MST avgFC achieve superior performance than GCNs with p -MST FC-of-avgROI, further supporting the previous inference that self-network connectivity makes a more positive contribution to GCN classification.



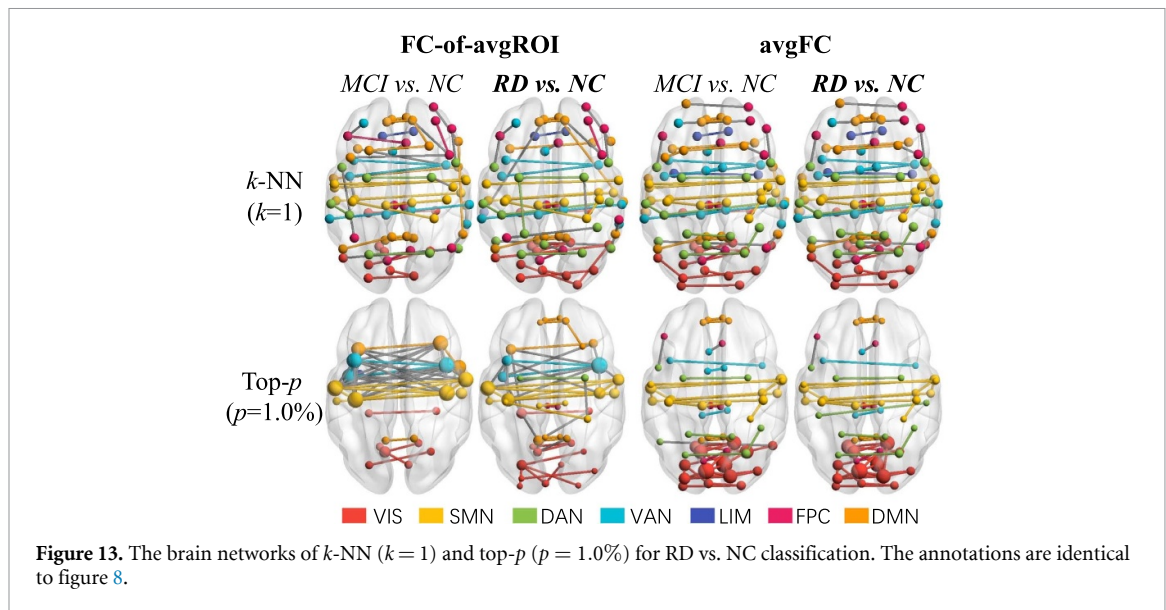
3.3. RD vs. NC classification results

To analysis the rfMRI data of dementia patient prior to clinical diagnosis, we perform the GCN classification of RD vs. NC for earlier prediction of dementia risk. Given our extensive analysis on MCI vs. NC classification, here we only conduct the RD vs. NC classification with k -NN graph when $k = 1$ and top- p graph when $p = 1.0\%$. Figure 12 depicts the results of the RD vs. NC classification. It can be observed that GNN with k -NN ($k = 1$) of the three type of graphs achieved better performance in the RD vs. NC classification, and obtained the best average accuracy of 78.8% with FC-of-avgROI graph when $k = 1$. This prove that GCN using global graphs with appropriate connectivity can achieve equivalent or superior performance to individual graphs. Besides, RD vs. NC classification exhibits decreased stability compared to MCI vs. NC classification, as indicated by a larger variance between the maximum and minimum values. This can potentially be attributed to a smaller amount of available training and test data for the RD vs. NC classification task.

From the brain networks for RD vs. NC classification in figure 13, it can be observed that there are more self-network connectivity of VIS in the FC-of-avgROI for RD vs. NC than that for MCI vs. NC, while there is little difference in the avgFC between the two kinks of classification. This implies that dementia may alter the brain networks in VIS. Besides, the avgFC exhibits more self-network connectivity in VIS and DMN compared to FC-of-avgROI in the top- p



($p = 1.0\%$) graphs. And the accuracy of GCN with top- p ($p = 1.0\%$) avgFC are higher than that of GCN with top- p ($p = 1.0\%$) FC-of-avgROI, suggesting that self-network connectivity in VIS and DMN positively contributes to GCN classification. This could explain why the accuracy of k -NN ($k = 1$) FC-of-avgFC is slightly higher than that of k -NN ($k = 1$) avgFC, as the former has similar or higher amount of self-network connectivity in VIS.



4. Discussion

In this study, we developed an FC based GCN framework for fMRI binary classifications and evaluated the performance on the longitudinal OASIS-3 dataset. We conducted two kinds of classification: MCI vs. NC (detecting MCI from NCs) and RD vs. NC (predicting dementia risk prior to clinical diagnosis of MCI). Besides, we explored the impact of different types and processing methods of FC on the GCN classification performance.

The results of our experiments revealed several important findings. First, our proposed GCN outperformed both the baseline GCN and SVM in terms of accuracy, indicating its effectiveness for MCI diagnosis and dementia risk prediction. The proposed GCN achieved the best average accuracy of 80.3% (11.7% higher than the baseline GCN and 23.5% higher than SVM) and the highest accuracy of 91.2%. This highlights the potential of deep learning techniques, specifically the GCN framework, for analyzing rfMRI data and detecting neurodegenerative disorders.

Second, we compared the effects of different types of FC utilized in the GCN, revealing that the topology of the brain network definitely affect the GCN classification performance. The comparison between absolute and non-absolute individual FC revealed that the proposed GCN with absolute individual FC performed slightly better. We compared the use of global FC matrices (avgFC and FC-of-avgROI) obtained from the training data with individual FC matrices from each rfMRI data. Nowadays, many studies believe that GCNs with individual connectivity matrices perform better than global connectivity matrices [23]. In this study, we found that the GCN framework with individual FC performed slightly better than that with global FC generally.

This suggests that individual-specific FC may contain valuable information for classification tasks, and incorporating them into the GCN model can improve its performance. However, GCN using global graphs with appropriate connectivity including self-network connectivity in VIS, DMN, VAN, and SMN—linked to disease symptoms or impairment—can achieve equivalent or superior performance to individual graphs in some cases. Besides, GCNs with avgFC or individual FC exhibit greater robustness compared with FC-of-avgROI as the number of edges in the graph increases.

Furthermore, we investigated different processing methods for FC matrices, including the *k*-NN graphs, threshold graphs, top-*p* graph and *p*-MST graphs. The results suggest that the choice of FC type and graph construction method can influence GCN classification performance. The GCN with *k*-NN graphs achieved the best average accuracy when *k* is set to 1, indicating that considering only the nearest neighbors in the graph can be beneficial for classification. The GCN with threshold graphs exhibited different patterns, with the accuracy varying with different threshold values. The results suggest that either excessive or extremely scarce connectivity can negatively affect the GCN classification performance. Besides, we investigated the use of top-*p* and *p*-MST graphs and found that utilizing fully-connected MST graphs in GCN yields better performance than top-*p* graphs with an equivalent edge percentage.

Lastly, we analyzed the functional brain networks utilized in the GCN framework for MCI or RD prediction, an aspect that has been scarcely explored in existing studies. We observed that between-network connectivity in the networks could negatively impact the GCN classification performance. This discovery aligns with the current research status that few studies have demonstrated significant associations between

disturbed self-network connectivity and cognitive impairments in MCI or AD [57]. Additionally, we found that graphs with a greater number of nodes with minimum self-network connectivity may contain more valuable information for the GCN classification. Besides, the comparison between MCI vs. NC and RD vs. NC implies that dementia may alter the brain networks in VIS and DMN at very early stage. The results indicates that the self-network connectivity in DMN, VIS, VAN and SMN may play a more significant role in GCN classification, suggesting that there might be topological impairments in these functional brain networks among MCI patients. These functional brain networks may have close connections to the symptoms of dementia such as diminished memory, disruptions in executive function, deficits in attention, visuospatial orientation, neuropsychiatric symptoms, etc. For instance, DMN is crucial for memory performance [52]; the visual cortex has been reported dysfunctional in AD [53]; VAN are considered to be responsible for the endogenous attention orienting process [54]; and SMN plays a pivotal role in episodic memory, action recognition and spatial navigation [55]. These findings are in line with the findings in [56] that disturbed FC of rest state was seen in the DMN and VIS in AD patients. Specially, the decreased self-network connectivity in DMN is often observed in rfMRI from the MCI and AD groups [57]. Li *et al* [53] found that both MCI and AD patients showed hyperactivation fell in FPC, VAN, DMN and SMN relative to NCs. Esposito *et al* [58] observed that rfMRI of MCI subjects showed increased intrinsic connectivity in the DMN and SMN. Zhang *et al* [59] revealed significant group-differed FC in VAN.

Our work has several limitations that warrant further investigation. Firstly, there is potential for improving the accuracy and computational efficiency of the proposed GCN. This could involve exploring alternative architectures, dynamic learning rate scheduling, and alternative activation functions, among other hyperparameter adjustments. Secondly, we only applied the GCN model to the fMRI data from the OASIS-3 dataset. In future work, we plan to generalize the model to different datasets and incorporate other multi-modality data, such as sMRI data, diffusion MRI data, and genetic information. Furthermore, the proposed GCN framework currently focuses on binary classification. However, dementia exists in different stages and severity levels. Therefore, it would be valuable to investigate the development of a multi-class classifier to capture the various levels of dementia. In this study, we utilized the Schaefer atlas to extract ROI-level connectivity. However, previous research has shown that the choice of brain atlas can impact the differentiation of various stages of dementia [60]. Therefore, it is important to explore the classification performance of our

model using other functional atlases and investigate the effects of self-network connectivity and between-network connectivity. Finally, even if we used a dataset of 1006 samples for NC vs. MCI classification and 282 samples for NC vs. RD classification, the proposed method might be limited by these numbers, as deep learning models rely on the use of a large number of samples to properly train and fit the huge set of parameters. Therefore, other databases with more samples should be investigated to corroborate our findings.

5. Conclusions

In this study, we developed an FC based GCN framework for fMRI binary classifications and conducted two kinds of classification on the longitudinal OASIS-3 dataset: MCI vs. NC (detecting MCI from NCs) and RD vs. NC (predicting dementia risk prior to clinical diagnosis of MCI). Besides, we explored how different types (individual FC, avgFC, FC-of-avgROI) and processing methods (k -NN, threshold, top- p and p -MST) of FC affect the GCN classification performance. The proposed GCN framework shows superior effectiveness compared with the baseline GCN and SVM. This work provides insights into the application of GCNs in brain analysis and early MCI detection, contributing to the understanding of MCI. The study holds significant potential for real-world applications, particularly in improving early clinical diagnosis and intervention for dementia and other neurodegenerative diseases.

Data availability statement

The data that support the findings of this study are openly available at the following URL/DOI: www.oasis-brains.org/.

Acknowledgments

This work was carried out as part of the doctoral programme in Experimental Sciences and Technology at the University of Vic—Central University of Catalonia. F D work was supported in part by the Tianjin Science and Technology Plan Project (No. 22PTZWHZ00040). C F C work was partially supported by Grants PICT 2020-SERIEA-00457 and PIP 112202101 00284CO (Argentina).

ORCID iDs

Zhe Sun  <https://orcid.org/0000-0002-6531-0769>

Cesar F Caiafa  <https://orcid.org/0000-0001-5437-6095>

Jordi Solé-Casals  <https://orcid.org/0000-0002-6534-1979>

References

- [1] Breijyeh Z and Karaman R 2020 Comprehensive review on Alzheimer's disease: causes and treatment *Molecules* **25** 5789
- [2] Srivastava S, Ahmad R and Kumar Khare S 2021 Alzheimer's disease and its treatment by different approaches: a review *Eur. J. Med. Chem.* **216** 113320
- [3] López O L and DEKOSKY S T 2008 Clinical symptoms in Alzheimer's disease *Handb Clin Neurol* **89** 207–16
- [4] Wee C-Y, Liu C, Lee A, Poh J S, Ji H and Qiu A (The Alzheimer's Disease Neuroimage Initiative) 2019 Cortical graph neural network for AD and MCI diagnosis and transfer learning across populations *NeuroImage Clin.* **23** 101929
- [5] Karakaya T, Fußer F, Schroder J and Pantel J 2013 Pharmacological treatment of mild cognitive impairment as a prodromal syndrome of Alzheimer's disease *Curr. Neuropharmacol.* **11** 102–8(7)
- [6] Robinson L, Tang E and Taylor J-P 2015 Dementia: timely diagnosis and early intervention *BMJ* **350** h3029
- [7] Chandra A, Dervenoulas G and Politis M 2019 Magnetic resonance imaging in Alzheimer's disease and mild cognitive impairment *J. Neurol.* **266** 1293–302
- [8] Liu S, Cai W, Liu S, Zhang F, Fulham M, Feng D, Pujol S and Kikinis R 2015 Multimodal neuroimaging computing: a review of the applications in neuropsychiatric disorders *Brain Inf.* **2** 167–80
- [9] Bi X, Zhao X, Huang H, Chen D and Ma Y 2020 Functional brain network classification for Alzheimer's disease detection with deep features and extreme learning machine *Cogn. Comput.* **12** 513–27
- [10] Greicius M D, Krasnow B, Reiss A L and Menon V 2003 Functional connectivity in the resting brain: a network analysis of the default mode hypothesis *Proc. Natl Acad. Sci.* **100** 253–8
- [11] Bullmore E and Sporns O 2009 Complex brain networks: graph theoretical analysis of structural and functional systems *Nat. Rev. Neurosci.* **10** 186–98
- [12] Illakiya T and Karthik R 2023 Automatic detection of Alzheimer's disease using deep learning models and neuro-imaging: current trends and future perspectives *Neuroinformatics* **21** 339–64
- [13] Warren S L and Moustafa A A 2023 Functional magnetic resonance imaging, deep learning and Alzheimer's disease: a systematic review *J. Neuroimaging* **33** 5–18
- [14] Zhang Y et al 2023 Machine learning-based identification of a psychotherapy-predictive electroencephalographic signature in PTSD *Nat. Mental Health* **1** 284–94
- [15] Borchert R J et al 2023 Artificial intelligence for diagnostic and prognostic neuroimaging in dementia: a systematic review *Alzheimer's Dementia* **19** 5885–904
- [16] Devika K and Ramana Murthy Oruganti V 2021 A machine learning approach for diagnosing neurological disorders using longitudinal resting-state fMRI 2021 *11th Int. Conf. on Cloud Computing, Data Science & Engineering (Confluence)* (IEEE) pp 494–9
- [17] Helaly H A, Badawy M and Haikal A Y 2022 Deep learning approach for early detection of Alzheimer's disease *Cogn. Comput.* **14** 1711–27
- [18] Ebrahimi-Ghahnavieh A, Luo S and Chiong R 2019 Transfer learning for Alzheimer's disease detection on MRI images 2019 *IEEE Int. Conf. on Industry 4.0, Artificial Intelligence and Communications Technology (IAICT)* (IEEE) pp 133–8
- [19] Zhao K, Duka B, Xie H, Oathes D J, Calhoun V and Zhang Y 2022 A dynamic graph convolutional neural network framework reveals new insights into connectome dysfunctions in ADHD *NeuroImage* **246** 118774
- [20] Niepert M, Ahmed M and Kutzkov K 2016 Learning convolutional neural networks for graphs *Int. Conf. on Machine Learning (PMLR)* pp 1014–23
- [21] Scarselli F, Gori M, Chung Tsoi A, Hagenbuchner M and Monfardini G 2008 The graph neural network model *IEEE Trans. Neural Netw.* **20** 61–80
- [22] Wein S 2023 Applications of spatio-temporal graph neural network models for brain connectivity analysis *PhD Thesis* University of Regensburg
- [23] Parisot S, Ira Ktena S, Ferrante E, Lee M, Guerrero Moreno R, Glocker B and Rueckert D 2017 Spectral graph convolutions for population-based disease prediction *Int. Conf. on Medical Image Computing and Computer-Assisted Intervention* (Springer) pp 177–85
- [24] Ira Ktena S, Parisot S, Ferrante E, Rajchl M, Lee M, Glocker B and Rueckert D 2018 Metric learning with spectral graph convolutions on brain connectivity networks *NeuroImage* **169** 431–42
- [25] Wang L, Li K and Hu X P 2021 Graph convolutional network for fMRI analysis based on connectivity neighborhood *Netw. Neurosci.* **5** 83–95
- [26] Tang H, Ma G, Guo L, Fu X, Huang H and Zhan L 2022 Contrastive brain network learning via hierarchical signed graph pooling model *IEEE Trans. Neural Netw. Learn. Syst.* **1**–13
- [27] Lei B et al 2023 Multi-scale enhanced graph convolutional network for mild cognitive impairment detection *Pattern Recognit.* **134** 109106
- [28] LaMontagne P J et al 2019 OASIS-3: longitudinal neuroimaging, clinical, and cognitive dataset for normal aging and Alzheimer's disease *medRxiv Preprint* <https://doi.org/10.1101/2019.12.13.19014902> (posted online 15 December 2019, accessed 15 February 2022)
- [29] Esteban O et al 2019 fMRIPrep: a robust preprocessing pipeline for functional MRI *Nat. Methods* **16** 111–6
- [30] Avants B B, Epstein C L, Grossman M and Gee J C 2008 Symmetric diffeomorphic image registration with cross-correlation: evaluating automated labeling of elderly and neurodegenerative brain *Med. Image Anal.* **12** 26–41
- [31] Zhang Y, Brady J M and Smith S 2000 Hidden Markov random field model for segmentation of brain MR image *Proc. SPIE* **3979** 1126–37
- [32] Greve D N and Fischl B 2009 Accurate and robust brain image alignment using boundary-based registration *NeuroImage* **48** 63–72
- [33] Pruim R H R, Mennes M, van Rooij D, Llera A, Buitelaar J K and Beckmann C F 2015 ICA-AROMA: a robust ICA-based strategy for removing motion artifacts from fMRI data *NeuroImage* **112** 267–77
- [34] Schaefer A, Kong R, Gordon E M, Laumann T O, Zuo Xi-N, Holmes A J, Eickhoff S B and Thomas Yeo B T 2018 Local-global parcellation of the human cerebral cortex from intrinsic functional connectivity MRI *Cereb. Cortex* **28** 3095–114
- [35] Cao M, Yang M, Qin C, Zhu X, Chen Y, Wang J and Liu T 2021 Using DeepGCN to identify the autism spectrum disorder from multi-site resting-state data *Biomed. Signal Process. Control* **70** 103015
- [36] Sólón Heinsfeld A, Franco A R, Craddock R C, Buchweitz A and Meneguzzi F 2018 Identification of autism spectrum disorder using deep learning and the ABIDE dataset *NeuroImage Clin.* **17** 16–23
- [37] Stam C J, Tewarie P, Van Dellen E, Van Straaten E C W, Hillebrand A and Van Mieghem P 2014 The trees and the forest: characterization of complex brain networks with minimum spanning trees *Int. J. Psychophysiol.* **92** 129–38
- [38] Alexander-Bloch A F, Gogtay N, Meunier D, Birn R, Clasen Liv, Lalonde F, Lenroot R, Giedd J and Bullmore E T 2010 Disrupted modularity and local connectivity of brain functional networks in childhood-onset schizophrenia *Front. Syst. Neurosci.* **4** 147
- [39] Zhou J, Cui G, Hu S, Zhang Z, Yang C, Liu Z, Wang L, Li C and Sun M 2020 Graph neural networks: a review of methods and applications *AI Open* **1** 57–81
- [40] Hanik M, Arif Demirtaş M, Amine Gharsallaoui M and Rekiq I 2022 Predicting cognitive scores with graph neural networks through sample selection learning *Brain Imaging Behav.* **16** 1123–38

- [41] Sporns O, Tononi G and Kötter R 2005 The human connectome: a structural description of the human brain *PLoS Comput. Biol.* **1** e42
- [42] Suprano I 2019 Cerebral connectivity study by functional and diffusion MRI in intelligence *PhD Thesis* Université de Lyon
- [43] Micheli A 2009 Neural network for graphs: a contextual constructive approach *IEEE Trans. Neural Netw.* **20** 498–511
- [44] Errica F, Podda M, Bacciu D and Micheli A 2020 A fair comparison of graph neural networks for graph classification *Int. Conf. on Learning Representations (ICLR 2020)*
- [45] Fey M and Eric Lenssen J 2019 Fast graph representation learning with PyTorch geometric *ICLR Workshop on Representation Learning on Graphs and Manifolds*
- [46] Morris C, Ritzert M, Fey M, Hamilton W L, Eric Lenssen J, Rattan G and Grohe M 2019 Weisfeiler and Leman go neural: higher-order graph neural networks *Proc. AAAI Conf. on Artificial Intelligence* vol 33 pp 4602–9
- [47] Nair V and Hinton G E 2010 Rectified linear units improve restricted Boltzmann machines *Proc. 27th Int. Conf. on Machine Learning (ICML-10)*
- [48] Kingma D P and Ba J L 2015 Adam: a method for stochastic optimization *Int. Conf. on Learning Representations* pp 1–13
- [49] Burges C J C 1998 A tutorial on support vector machines for pattern recognition *Data Min. Knowledge Discovery* **2** 121–67
- [50] Xia M, Wang J and He Y 2013 Brainnet viewer: a network visualization tool for human brain connectomics *PLoS One* **8** e68910
- [51] Buckner R L, Krienen F M, Castellanos A, Diaz J C and Thomas Yeo B T 2011 The organization of the human cerebellum estimated by intrinsic functional connectivity *J. Neurophysiol.* **106** 2322–45
- [52] He J, Carmichael O, Fletcher E, Singh B, Iosif A-M, Martinez O, Reed B, Yonelinas A and DeCarli C 2012 Influence of functional connectivity and structural MRI measures on episodic memory *Neurobiol. Aging* **33** 2612–20
- [53] Li H-J, Hou X-H, Liu H-H, Yue C-L, He Y and Zuo Xi-N 2015 Toward systems neuroscience in mild cognitive impairment and Alzheimer's disease: a meta-analysis of 75 fMRI studies *Hum. Brain Mapp.* **36** 1217–32
- [54] Corbetta M and Shulman G L 2002 Control of goal-directed and stimulus-driven attention in the brain *Nat. Rev. Neurosci.* **3** 201–15
- [55] Russ M O, Mack W, Grama C-R, Lanfermann H and Knopf M 2003 Enactment effect in memory: evidence concerning the function of the supramarginal gyrus *Exp. Brain Res.* **149** 497–504
- [56] Zheng W, Liu X, Song H, Li K and Wang Z 2017 Altered functional connectivity of cognitive-related cerebellar subregions in Alzheimer's disease *Front. Aging Neurosci.* **9** 143
- [57] Zhu H et al 2016 Changes of intranetwork and internetwork functional connectivity in Alzheimer's disease and mild cognitive impairment *J. Neural Eng.* **13** 046008
- [58] Esposito R, Mosca A, Pieramico V, Cieri F, Cera N and Sensi S L 2013 Characterization of resting state activity in MCI individuals *PeerJ* **1** e135
- [59] Zhang Z, Zheng H, Liang K, Wang H, Kong S, Hu J, Wu F and Sun G 2015 Functional degeneration in dorsal and ventral attention systems in amnesic mild cognitive impairment and Alzheimer's disease: an fMRI study *Neurosci. Lett.* **585** 160–5
- [60] Wu Z, Dong X and Potter T 2019 Yingchun Zhang and Alzheimer's disease neuroimaging initiative. Effects of brain parcellation on the characterization of topological deterioration in Alzheimer's disease *Front. Aging Neurosci.* **11** 113